Ultra-wideband radar imaging using a hybrid of Kirchhoff migration and stolt F-K migration with an inverse boundary scattering transform

Sakamoto, T; Sato, T; Aubry, PJ; Yarovoy, A

DOI
10.1109/TAP.2015.2431725

Publication date
2015

Document Version
Accepted author manuscript

Published in
IEEE Transactions on Antennas and Propagation

Ultra-Wideband Radar Imaging using a Hybrid of Kirchhoff Migration and Stolt F-K Migration with an Inverse Boundary Scattering Transform

Takuya Sakamoto, *Member, IEEE* Toru Sato, *Member, IEEE*
Pascal J. Aubry, and Alexander G. Yarovoy, *Senior Member, IEEE*

***Abstract*—In this paper, we propose a fast and accurate radar imaging algorithm that combines Kirchhoff migration with Stolt's frequency-wavenumber (F-K) migration. F-K migration is known as a fast imaging method in the F-K domain, while Kirchhoff migration is reported to be more accurate. However, Kirchhoff migration requires the reflection points to be located as a function of the antenna position and the delay time. This prevents the use of fast Fourier transforms because Kirchhoff migration must be processed in the time domain, and this can be extremely time-consuming. The proposed algorithm overcomes this hurdle by introducing the texture angle and the inverse boundary scattering transform. These two tools enable the locations of the reflection points to be determined rapidly for each pixel of a radar image. The radar signals are then modified according to the Kirchhoff integral, before Stolt F-K migration is applied in the frequency domain to produce an accurate radar image. To demonstrate the performance of the proposed method, the conventional delay-and-sum (DAS) migration, Kirchhoff migration, Stolt F-K migration, and the proposed method are applied to the same measured datasets.**

***Index Terms*—ultra-wideband, radar imaging, Stolt F-K migration, Kirchhoff migration, inverse boundary scattering transform**

I. Introduction

ULTRA-WIDEBAND (UWB) radar imaging is of great importance to a wide variety of applications, including sensor networks [1], through-the-wall imaging [2], [3], breast tumor detection [4], and ground penetrating radar [5]. Certain applications, such as security systems, require the imaging process to be both accurate and fast. Using the Kirchhoff integral, Zhuge et al. [6] proposed an imaging algorithm that generates clearer images than the conventional delay-and-sum (DAS) migration process. However, the Kirchhoff migration must be computed in the time-domain, which makes the imaging process rather time-consuming. Because many imaging systems require real-time processing, this drawback hinders the practical application of this method.

Stolt's frequency-wavenumber (F-K) migration is known to be a fast imaging method, and has been studied in numerous works in the literature [7], [8], [9]. The method uses back-projection in the F-K domain, meaning that Stolt F-K migration is basically the same as DAS migration [10]. However, when calculating the fast Fourier transform (FFT), the edges are suppressed by a roll-off window, and this inevitably leads to some information loss. Therefore, the imaging capability of Stolt F-K migration is, in general, slightly inferior to that of DAS migration.

To overcome these difficulties, this paper presents a new method whereby Kirchhoff migration and Stolt F-K migration are combined. The problem with Kirchhoff migration is that it requires prior knowledge of reflection-point locations for each pixel of the radar image. This has previously prevented its use with Stolt F-K migration, because the target reflection points are unknown. The target reflection points must first be calculated in the time domain, and then Stolt F-K migration can be applied. Thus, in this paper, we introduce essential tools: the texture angle and the inverse boundary scattering transform (IBST). These tools allow us to modify the signals in the time domain so that they have the same form as the Kirchhoff integrand. Then, the modified signals can be transformed to the F-K domain to be processed using Stolt F-K migration. Because the texture angle and IBST calculations are fast, these additional processes do not affect the computation speed of Stolt F-K migration. The proposed method is also shown to generate high-quality images. The performance of the proposed method is confirmed by applying conventional DAS migration, Kirchhoff migration, Stolt F-K migration, and the proposed method to the scattering data from a corner reflector, and five different targets: a knife, a laser measure, a handgun, a bottle of water, and a set of keys. The results demonstrate the high-quality imaging capabilities of the proposed method.

II. System Model

The measurement system consists of a pair of antennas (transmitter and receiver) positioned in the $z = 0$ plane in the x direction at a fixed separation of $2d$. The midpoint between the transmitter and the receiver is denoted by $(X, Y, 0)$. Therefore, the transmitter and the receiver are located at $\boldsymbol{r}_1 = (X-d, Y, 0)$ and $\boldsymbol{r}_2 = (X+d, Y, 0)$, respectively. When the transmitter-receiver pair is scanning at discrete intervals across a region of the $z = 0$ plane, UWB pulses are transmitted and the pulse echoes are received. Figure 1 shows the system setup that has been assumed in this paper.

The received signals contain both echoes from the target and a coupling signal that propagates directly from transmitter

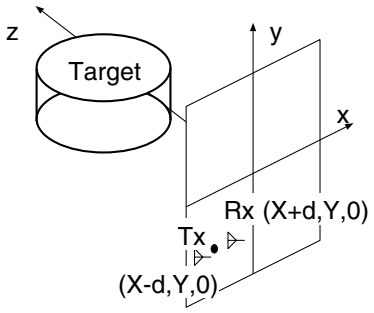

Fig. 1. System setup with antennas scanning from the x-y plane.

to receiver. To eliminate this coupling signal, the background signal, which is measured without a target prior to the actual measurements, is subtracted from the received signal. Given that the antennas' midpoint is $(X, Y, 0)$, the received signal is labeled $s(X, Y, Z)$, where $Z = ct/2$. Here, c is the speed of the electromagnetic wave, and t is the time interval between transmission and reception of the signal.

III. Stolt F-K Migration

Stolt F-K migration is a fast imaging algorithm that uses the fast Fourier transform (FFT) algorithm in the F-K domain. Let $\Phi(x, y, z, t)$ be a wavefield at a point (x, y, z) and time t, and let $\phi(k_x, k_y, z, \omega)$ be a three-dimensional Fourier transform in terms of x, y, and t. This wavefield satisfies the Helmholtz equation

$$\nabla^2\phi + k_0^2\phi = 0, \tag{1}$$

which can be also written as

$$\frac{\partial^2}{\partial z^2}\phi + \hat{k}_z^2\phi = 0. \tag{2}$$

Here, $k_0 = \omega/c$ and $\hat{k}_z = \sqrt{k_0^2 - k_x^2 - k_y^2}$ is the effective wavenumber in the z-direction, assuming that the wave is a plane wave. Equation (2) indicates that ϕ is approximated as a wave propagating in the z-direction with the wavenumber $\hat{k}_z$.

If the wavefield is observed at all points in the x-y plane, i.e., if $\Phi(x, y, 0, t)$ are known, then the target image to be estimated corresponds to $\Phi(x, y, z, 0)$. If the definition of $t = 0$ is suitably chosen, this can then be expressed as

$$\Phi(x, y, z, 0) = \int \phi(k_x, k_y, 0, \omega)\mathrm{e}^{\mathrm{j}(k_x x + k_y y + \hat{k}_z z)}\mathrm{d}k_x\mathrm{d}k_y\mathrm{d}\omega. \tag{3}$$

Using $\hat{k}_z$ to express ω as

$$\omega = c \cdot \mathrm{sign}(\hat{k}_z)\sqrt{k_x^2 + k_y^2 + \hat{k}_z^2}, \tag{4}$$

Eq. (3) can then be written as

$$\Phi(x, y, z, 0) = \int \frac{c\hat{k}_z}{\sqrt{k_x^2 + k_y^2 + \hat{k}_z^2}}\phi(k_x, k_y, 0, \omega) \cdot\mathrm{e}^{\mathrm{j}(k_x x + k_y y + \hat{k}_z z)}\mathrm{d}k_x\mathrm{d}k_y\mathrm{d}k_z, \tag{5}$$

where the first term of the integrand is the Jacobian determinant produced by the change of variables from ω to $\hat{k}_z$. Importantly, Eq. (5) can be solved by applying the inverse FFT (IFFT) to the re-sampled data in the form

$$\Phi(x, y, z) = \mathcal{F}_{k_x}^{-1}\mathcal{F}_{k_y}^{-1}\mathcal{F}_{\hat{k}_z}^{-1}\psi(k_x, k_y, \hat{k}_z), \tag{6}$$

$$\psi(k_x, k_y, \hat{k}_z) = \frac{c\hat{k}_z}{\sqrt{k_x^2 + k_y^2 + \hat{k}_z^2}}\phi(k_x, k_y, 0, \omega(k_x, k_y, \hat{k}_z)), \tag{7}$$

where ω is given explicitly as a function of k_x, k_y, and $\hat{k}_z$. While the FFT enables fast computation of the Stolt F-K migration, it is known that the imaging quality offered by this method is inferior to that based on Kirchhoff migration.

IV. Kirchhoff Migration

In Dirichlet problems, the Kirchhoff integral is known to be an exact expression of a scalar wave-field [11]. This knowledge is used in Kirchhoff migration to generate high-quality images. Assuming that we know the wave-field at a receiver position at $\boldsymbol{r}'$ located on a closed surface S, the wave-field at an arbitrary point $\boldsymbol{r}$ inside S can be calculated using the Kirchhoff integral. The Kirchhoff integral for a wave-field $\Phi(\boldsymbol{r}, t) = \Phi(x, y, z, t)$ is expressed as

$$\Phi(\boldsymbol{r}, t) = \frac{1}{4\pi}\oint_S \left\{\frac{1}{R}\frac{\partial}{\partial n}\Phi(\boldsymbol{r}', t + \tau') - \frac{\partial}{\partial n}\frac{1}{R}\Phi(\boldsymbol{r}', t + \tau') + \frac{1}{cR}\frac{\partial R}{\partial n}\frac{\partial}{\partial t}\Phi(\boldsymbol{r}', t + \tau')\right\}\mathrm{d}S, \tag{8}$$

where $\boldsymbol{r} = (x, y, z)$ is a point inside the closed region bounded by surface S, $\boldsymbol{r}'$ is a point on the surface S, $R = |\boldsymbol{r} - \boldsymbol{r}'|$, $\tau' = R/c$, and $\partial/\partial n$ denotes the spatial derivative in the direction of the vector normal to S. Given the appropriate surface information about the wave-field, its value at $\boldsymbol{r}$ can be calculated using Eq. (8).

Zhuge et al. [6] proposed an imaging algorithm, based on a multiple-input multiple-output (MIMO) radar model. They calculated the Kirchhoff migration image using double integrals over the transmitter and receiver scan surfaces. While the present study assumes the use of a single-input single-output (SISO) radar system that uses a pair of antennas with a fixed spacing, the same formula is applicable. In our system, the transmitter and receiver are located at $\boldsymbol{r}_1$ and $\boldsymbol{r}_2$, respectively, with a midpoint of $\boldsymbol{r}_0$ at a fixed spacing $2d$ in the x-direction. Let us redefine the raw signal $s_0(\boldsymbol{r}_0, t)$ that is transmitted and received at $\boldsymbol{r}_1 = \boldsymbol{r}_0 - \boldsymbol{d}$ and $\boldsymbol{r}_2 = \boldsymbol{r}_0 + \boldsymbol{d}$, respectively, where $\boldsymbol{d} = (d, 0, 0)$. This raw signal can also be expressed using $s(X, Y, Z)$, which was introduced in the second section as $s_0(\boldsymbol{r}_0, t) = s(X, Y, Z)$, if $\boldsymbol{r}_0 = (X, Y, 0)$ and $Z = ct/2$ are satisfied. The Kirchhoff migration can be performed by integrating the signals to obtain the image $I(\boldsymbol{r})$ in the form

$$
\begin{aligned}
I(\boldsymbol{r}) &= \int_S \frac{\partial R_1}{\partial n}\frac{\partial R_2}{\partial n}\frac{1}{R_1 R_2} \\
&\cdot \left\{ \frac{1}{c^2}\frac{\partial^2}{\partial t^2} s_0(\boldsymbol{r}_0, t+\tau) \right. \\
&+ \frac{1}{c}\left(\frac{1}{R_1}+\frac{1}{R_2}\right)\frac{\partial}{\partial t} s_0(\boldsymbol{r}_0, t+\tau) \\
&+ \left. \frac{1}{R_1 R_2} s_0(\boldsymbol{r}_0, t+\tau) \right\} \mathrm{d}S \Big|_{t=0}, \qquad (9)
\end{aligned}
$$

where S is the antenna scanning plane $z=0$, $R_1 = |\boldsymbol{r}-\boldsymbol{r}_1|$, $R_2 = |\boldsymbol{r}-\boldsymbol{r}_2|$, $\tau = (R_1+R_2)/c$, and $\partial/\partial n$ denotes the spatial derivatives normal to the surface S. Equation (9) indicates that the Kirchhoff migration is performed based on a single integral, unlike the formula proposed in [6].

The integral in Eq. (9) can be readily calculated in the space-time domain as reported in [6]. This is because the region of interest is divided into numerous voxels, and we can calculate all necessary coefficients, such as R_1 and R_2 in Eq. (9), for each of these voxels without estimating the actual target position. This method is called Kirchhoff migration in the remainder of this paper.

Note here that Eq. (9) can be converted to the frequency domain by implementation of the appropriate frequency domain kernel, as seen in the diffraction tomographic algorithm [12]. This paper provides an alternative approach to this problem by using a fundamentally different principle. It will be an important part of our future studies to compare the image resolutions and computational speeds achieved using the diffraction tomographic algorithm and the algorithm proposed in this paper.

V. Inverse Boundary Scattering Transform and Texture Angles

We have developed a fast radar imaging algorithm (SEABED, or shape estimation algorithm based on the boundary scattering transform and extraction of directly scattered waves) that uses the IBST. The IBST is a transform that is reversible between a target shape and the corresponding echo data [13], [14], [15], [16], [17]. Because the IBST describes a one-to-one correspondence, SEABED does not require any iterative or repetitive processing, and thus enables fast imaging. Another advantage of SEABED is that, unlike conventional methods, a target location is estimated for each radar image pixel. In this study, we exploit this characteristic to develop a new algorithm.

A radar image can be obtained using the following IBST [18], which is applied to the signal $s(X,Y,Z)$:

$$
\begin{aligned}
x &= X - \frac{2Z^3 Z_X}{Z^2 - d^2 + \sqrt{(Z^2-d^2)^2 + 4d^2 Z^2 Z_X^2}}, \qquad (10) \\
y &= Y + Z_Y \left\{ d^2 (x-X)^2 - Z^4 \right\} / Z^3, \qquad (11) \\
z &= \sqrt{Z^2 - d^2 - (y-Y)^2 - \frac{(Z^2-d^2)(x-X)^2}{Z^2}} \qquad (12)
\end{aligned}
$$

where, for simplicity, $Z_X = \partial Z/\partial X$ and $Z_Y = \partial Z/\partial Y$. In the original SEABED, the signal peaks are extracted, and the IBST is applied to these peaks. However, in this study, we require the target locations that correspond to all the pixels in the radar image.

We introduce the texture angle for radar images to estimate the derivatives Z_X and Z_Y that are required in Eqs. (10) and (11). The texture angle was originally proposed for the estimation of target speeds from radar signals [19], [20]. We use the same concept but for a different purpose: we define the texture angle of a radar signal $s(X,Y,Z)$ as

$$
\begin{aligned}
\theta_X(X,Y,Z) &= \tan^{-1}\left(\frac{\partial s(X,Y,Z)/\partial X}{\partial s(X,Y,Z)/\partial Z} \right), \qquad (13) \\
\theta_Y(X,Y,Z) &= \tan^{-1}\left(\frac{\partial s(X,Y,Z)/\partial Y}{\partial s(X,Y,Z)/\partial Z} \right). \qquad (14)
\end{aligned}
$$

The derivatives Z_X and Z_Y that are needed for the IBST are estimated using these values θ_X and θ_Y.

Let us assume that $s(X,Y,Z)$ can be approximated as $s(X,Y,Z) = p(Z - Z_0(X,Y))$ with the arbitrary function $p(\cdot)$, which means that the signal has a local equiphase surface $Z = Z_0(X,Y)$. Under this assumption, we obtain $\partial s/\partial X = -p'(Z - Z_0(X,Y))\partial Z_0/\partial X$, $\partial s/\partial Y = -p'(Z - Z_0(X,Y))\partial Z_0/\partial Y$, and $\partial s/\partial Z = p'(Z - Z_0(X,Y))$. Therefore, $Z_X = \partial Z_0/\partial X$ and $Z_Y = \partial Z_0/\partial Y$ can be obtained by calculating $Z_X = -\tan(\theta_X)$ and $Z_Y = -\tan(\theta_Y)$. Using these results, we can estimate the target position (x,y,z) using Eqs. (10-12). The texture angles θ_X and θ_Y correspond to the angles of stripes that appear in the X-Z and Y-Z planes, as will be shown in a later section. These stripes are intersections of the equiphase surface Z with XoZ or YoZ planes.

Next, the estimated target position (x,y,z) is used to calculate

$$
\begin{aligned}
R_1 &= \sqrt{(x-X+d)^2 + (y-Y)^2 + z^2}, \qquad (15) \\
R_2 &= \sqrt{(x-X-d)^2 + (y-Y)^2 + z^2} \qquad (16)
\end{aligned}
$$

and $\partial R_1/\partial n = z/R_1$. $\partial R_2/\partial n = z/R_2$. These values are then substituted into the following equation to give the modified Kirchhoff signal:

$$
\begin{aligned}
s'_{\mathrm{m}}(\boldsymbol{r}_0, t) &= \frac{\partial R_1}{\partial n}\frac{\partial R_2}{\partial n}\frac{1}{R_1 R_2} \\
&\cdot \left\{ \frac{1}{c^2}\frac{\partial^2}{\partial t^2} s(\boldsymbol{r}_0, t) + \frac{1}{c}\left(\frac{1}{R_1}+\frac{1}{R_2}\right)\frac{\partial}{\partial t} s(\boldsymbol{r}_0, t) \right. \\
&\left. + \frac{1}{R_1 R_2} s(\boldsymbol{r}_0, t) \right\}. \qquad (17)
\end{aligned}
$$

Finally, as proposed in [6], we can compensate for the propagation path loss using $s_{\mathrm{m}} = R_1^2 R_2^2 s'_{\mathrm{m}}$. Kirchhoff migration can then be realized by simply applying a conventional migration to the modified Kirchhoff signal $s_{\mathrm{m}}(\boldsymbol{r}_0, t)$ rather than the original signal $s(\boldsymbol{r}_0, t)$. This can be calculated using the FFT in exactly the same manner as it was used for Stolt F-K migration. The use of texture angles and the IBST allows us to use Stolt F-K migration and Kirchhoff migration simultaneously, which means that we can obtain high-quality images in a short time. We only use the texture angle and the IBST in our proposed hybrid method, and not in other conventional methods.

VI. Proposed Method

In this section, the actual procedure used for the proposed method is explained.

1) Calculate the texture angles $\theta_X(X_i, Y_i, Z_i)$ and $\theta_Y(X_i, Y_i, Z_i)$ using Eqs. (13) and (14), respectively, for each data sample $s(X_i, Y_i, Z_i)$ $(i = 1, 2, \cdots, N)$, where N is the number of data points and is defined as $N = N_X N_Y N_t$. Here, N_X and N_Y are the numbers of measurement points in the x and y directions, respectively, and N_t is the number of time samples.
2) Obtain the partial derivatives $Z_X = \tan(\theta_X)$ and $Z_Y = \tan(\theta_Y)$, and apply the IBST as per Eqs. (10)-(12) to calculate the target position (x_i, y_i, z_i) for the i-th data sample.
3) Calculate $\partial R/\partial n$ for each estimated reflection point (x_i, y_i, z_i).
4) Generate the modified Kirchhoff signals $s_m(X_i, Y_i, Z_i)$ using Eq. (17).
5) Apply the three-dimensional FFT to the modified Kirchhoff signal to obtain $\phi(k_x, k_y, \omega)$.
6) Obtain $\psi(k_x, k_y, k_z)$ using Eqs. (4) and (7).
7) Apply the three-dimensional IFFT as per Eq. (6) to obtain the final radar image.

Before application of the FFT and the IFFT, we apply a Hann window, which is also called a raised cosine window, to suppress undesired components caused by truncation of data. This means that we apply a three-dimensional Hann window twice in the calculation of the Kirchhoff migration and the proposed method. In the paper, the roll-off factor $0 \leq \alpha \leq 1$ of the window is set to 0.3, where a window with $\alpha = 1$ corresponds to a raised cosine window. The effect of α on the image resolution will be discussed in Section IX.

VII. Measurement of the Point Spread Functions of the Conventional and Proposed Methods

In this section, we apply the proposed method, along with conventional DAS migration, Kirchhoff migration, and Stolt F-K migration, to a dataset measured from a trihedral corner reflector acting as a target for estimation of an approximate point spread function (PSF), which is often used as an indicator of radar imaging capability. Assuming the linearity that a radar image can be approximated as the convolution of the actual target shape and the PSF, we can then assess the general radar imaging performance. For comparison, we also apply conventional DAS migration, Stolt F-K migration and Kirchhoff migration to the same dataset.

The datasets were measured in the frequency domain using a network analyzer (PNA E8364B, Agilent Technologies, CA, USA) to sweep 161 points at frequencies from 4.0 to 20.0 GHz. Before applying the imaging algorithms, the measured datasets were converted into time-domain data with 1000 samples for $0 \leq t \leq 6.3$ ns with a sampling interval of 6.3 ps, which corresponds to the maximum range of 94.5 cm in a mono-static radar configuration. Two Vivaldi antennas were used with $2d = 5.5$ cm antenna separation. Both antennas were vertically polarized. The antenna pair scanned in the X-Y plane ($Z = 0$) from $X_{\min} \leq X \leq X_{\max}$ and $Y_{\min} \leq Y \leq Y_{\max}$ at intervals of $\Delta_{X,Y}$, where $\Delta_{X,Y} = 1.0$ cm and $X_{\min}, X_{\max}, Y_{\min}$ and $Y_{\max}$ are -25.0, 25.0, -25.0 and 25.0 cm, respectively. Thus, the total number of measurement points was $51 \times 51 = 2601$. The position $(X, Y, 0)$ is defined as the midpoint between the transmitting and receiving antennas, which were located at $(X + d, Y, 0)$ and $(X - d, Y, 0)$, where $d = 2.75$ cm. The transmitted power was 2.0 dBm.

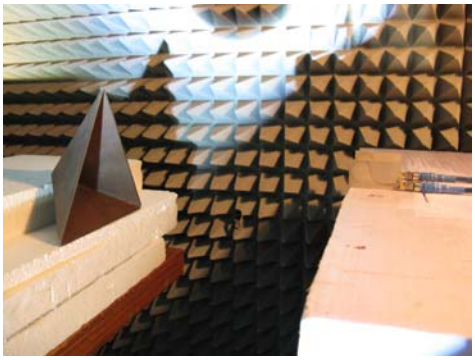

Fig. 2. Photograph of the trihedral corner reflector that was measured using the two Vivaldi antennas.

The target was a trihedral corner reflector with 13.0 cm sides and an apex that was placed at $(x, y, z) = (0.0\text{cm}, -2.0\text{cm}, 50.0\text{cm})$, which lies 50.0 cm from the antenna scanning plane ($z = 0$). Fig. 2 shows the measurement setup of the trihedral corner reflector using the two Vivaldi antennas. The trihedral corner reflector has three corners and one virtual scattering center point, which is located at its apex. Because the scattering from the corners of the reflector is much weaker than the scattering from the virtual scattering center, we only consider the focus size of the image of the virtual scattering center. The image produced by the application of imaging algorithms to the trihedral corner reflector dataset can therefore be considered approximately to be a PSF.

The images that were produced using DAS migration, Kirchhoff migration, Stolt F-K migration and the proposed method are shown in Fig. 3. We see that the images generated by DAS migration and Kirchhoff migration have higher sidelobes caused by data truncation at the edges of the measurement surface. In contrast, the images that were processed in the F-K domain have lower sidelobes because the Hann window was applied during their processing, as was mentioned in the previous section. Nevertheless, the main lobe of the Kirchhoff migration image is narrower than those of the others. The main lobe of the Stolt F-K migration image is as wide as that of the DAS migration image, whereas the proposed method produces an image with a relatively narrow main lobe and without dominant sidelobes.

The sections of these images along the x-axis are shown in Fig. 4. The PSF widths at -10 dB are 2.75, 2.29, 2.66, and 2.55 cm for the DAS migration, Kirchhoff migration, Stolt F-K migration and the proposed method, respectively. The Kirchhoff migration has a 20 % narrower PSF than the DAS migration, whereas the PSF of the proposed method is 8% narrower than the DAS migration's PSF. The Kirchhoff migration has the narrowest PSF. The DAS migration and

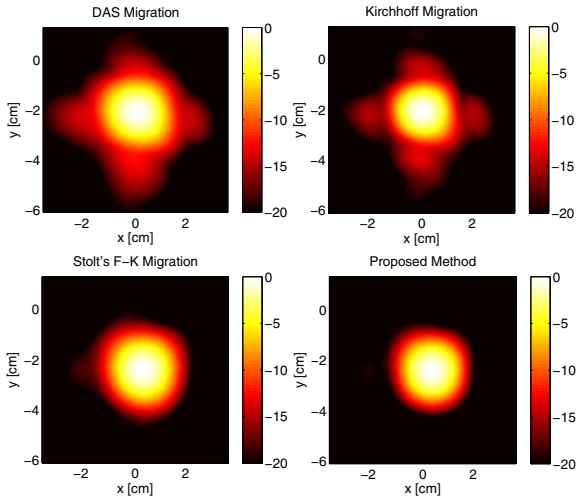

Fig. 3. Images generated using DAS migration (upper left), Kirchhoff migration (upper right), Stolt F-K migration (bottom left), and the proposed method (bottom right). The images are all in decibels.

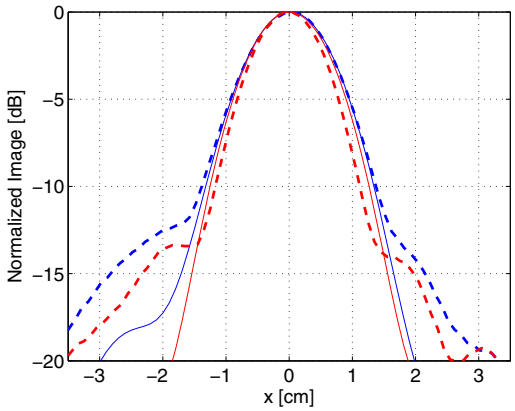

Fig. 4. Image sections along the x-axis for the DAS migration (dashed blue), Stolt's F-K migration (solid blue), the Kirchhoff migration (dashed red), and the proposed method (solid red).

Stolt F-K migration produce almost the same PSFs, which was also observed by Gilmore et al. [10]. The PSF of the proposed method lies between those of the Kirchhoff migration and the DAS migration. This is because the modified Kirchhoff signals generated by the proposed method cannot completely reproduce the integrand of the Kirchhoff integral because of the inaccurate estimation of the reflection points. It should be noted that the PSF is only one way to assess the imaging capability, and the PSF does not take into account the fact that the actual imaging algorithms often include nonlinear procedures. Therefore, these imaging algorithms must be investigated further by applying them to data that were measured for more complicated target shapes, as shown in the next section.

Fig. 5. Photograph of the five targets used in the measurements.

VIII. Imaging of Various Objects using the Conventional and Proposed Methods

In this section, we apply the four different imaging algorithms to radar echo datasets to study the performances of these algorithms in a more realistic scenario. The measurements were performed in the same way as those in the previous section, but with a larger measurement area where $X_{\min}, X_{\max}, Y_{\min}$ and $Y_{\max}$ are -37.0, 37.0, -37.0 and 37.0 cm, respectively. Thus, the total number of measurement points is $75 \times 75 = 5625$. For our measurements, five targets (a knife, a laser measure, a handgun, a bottle of water, and a set of keys) were fixed to a styrene foam board that was placed 60.0 cm away from the antenna scanning plane (see Fig. 5). Note that the back sides of these targets were attached to the board, which means that the actual reflection points of the targets are not the same, but are spread from 52.5 cm (the bottle of water) to 59.5 cm (the keys).

Figure 6 shows the signals that were received for $X = -13$ cm. We selected this slice for display because the signals for $X = -13$ cm contain overlapping echoes from three large targets: a knife, a handgun and a bottle of water. By incoherent integration of these unprocessed signals in terms of the delay path Z from $Z_1 = 52.5$ cm to $Z_2 = 59.5$ cm as

$$I_0 = \int_{Z_1}^{Z_2} |s(X, Y, Z)|^2 \, dZ, \tag{18}$$

we obtain the vague image that is shown in Fig. 7. Although the water bottle is almost visible on the bottom left, the unprocessed signals do not provide sufficiently accurate information about the target shapes.

By applying Eqs. (13) and (14) to the signals, we obtain the texture angle image (see Fig. 8). The texture angle shown in the figure corresponds to the angle of wavefronts relative to the vertical axis in Fig. 6, and it should be also noted that the horizontal and vertical axes are not to the same scale in the figure. Next, we use Eqs. (10), (11), and (12) to obtain the target positions (x, y, z) for each pixel in the image. The image that was estimated using the texture angle and the IBST is shown in Fig. 9. Although the actual image is three-dimensional (3D), the 3D image is projected onto x-y plane

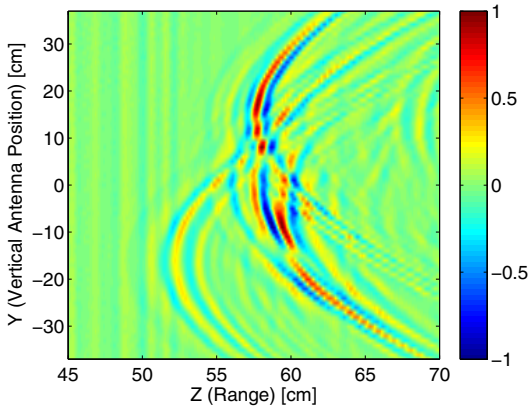

Fig. 6. The raw signals received for $X = -13$ cm.

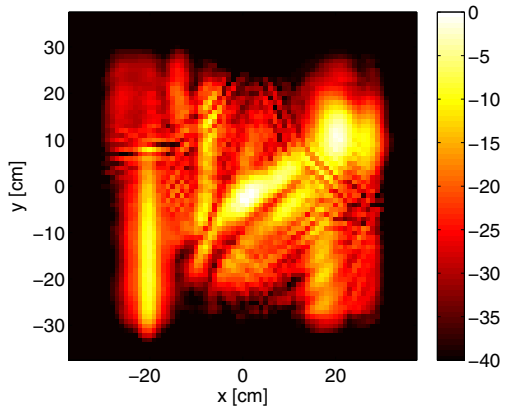

Fig. 7. Unprocessed data intensities corresponding to the ranges of the targets (in decibels).

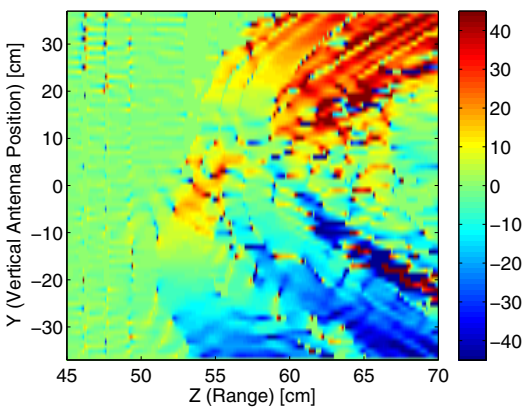

Fig. 8. Texture angles obtained from the data in Fig. 6 (in degrees).

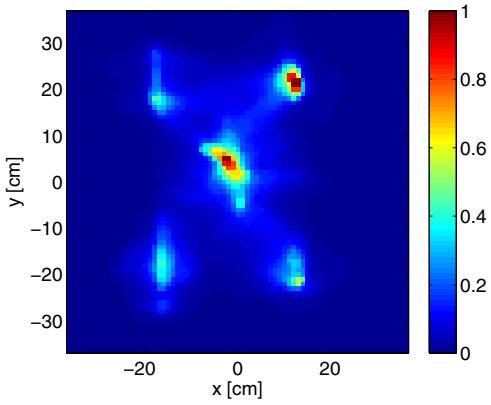

Fig. 9. Target positions estimated using texture angles and the IBST.

to generate this image. The physical quantity displayed in this image corresponds to the back-projected vertical component of the scattered electric field.

In Fig. 9, each target image is blurred, and some artifacts are seen between the target images. The image is produced using a combination of the texture angle and IBST, and is not very accurate, and it is limited by the fact that only one target position is given for each data sample $s(X, Y, Z)$. In actual signals, however, multiple echoes from different targets can be received at the same time and at the same position. This possibility is not considered when calculating the texture angle; a dominant signal can mask other weaker signals, and thus leads to information loss. This is why our proposed algorithm is required for further processing of the data to obtain clearer images.

We must note here that the image produced using IBST is not a conventional radar image, but each data sample (X, Y, Z) is associated with one of the voxels in the 3D image. This characteristic enables us to calculate the modified Kirchhoff signals, as shown in Fig. 10. We see that, when compared with the signals shown in Fig. 6, the higher frequency components are enhanced in this image. The red dashed line and black solid line in Fig. 11 show the power spectrum densities of the original and modified Kirchhoff signals, respectively, which clearly shows the enhancement of high frequency components in the modified Kirchhoff signal. Finally, the Stolt F-K migration algorithm is applied to the modified Kirchhoff signals to obtain the target image.

For comparison, we apply the proposed method along with

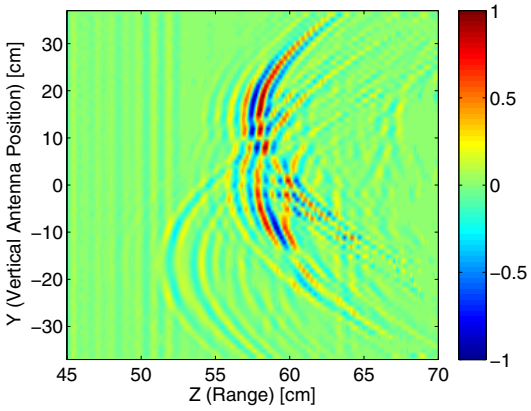

Fig. 10. Modified Kirchhoff signals obtained from the data that was used for Fig. 6.

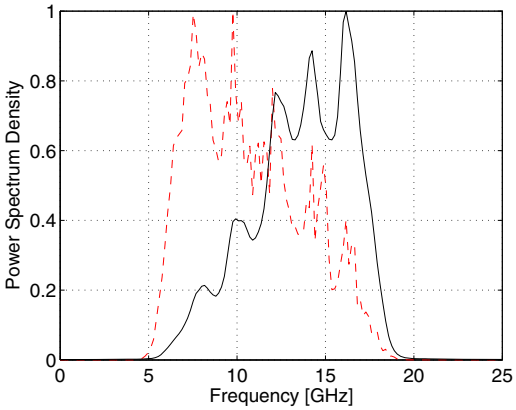

Fig. 11. Power spectrum densities of the original signal (in red) and the modified Kirchhoff signal (in black).

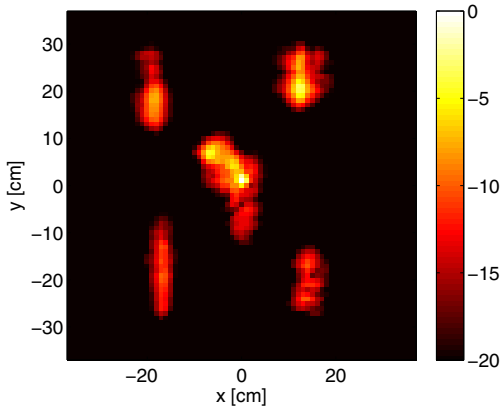

Fig. 13. Image generated using time-domain Kirchhoff migration (in decibels). The computation time was 1148.8 s.

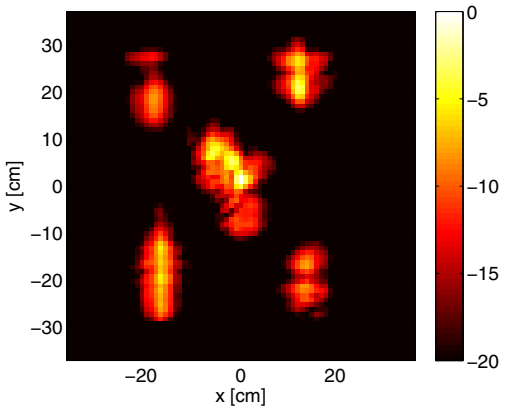

Fig. 12. Image generated using DAS migration (in decibels). The computation time was 1119.3 s.

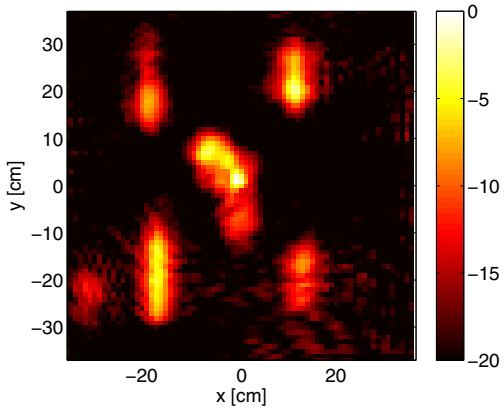

Fig. 14. Image generated using Stolt F-K migration (in decibels). The computation time was 2.48 s.

conventional DAS migration, Kirchhoff migration, and Stolt F-K migration. For this purpose, each 3-D image $I(x, y, z)$ was generated inside the same cuboid for $x_{\min} \leq x \leq x_{\max}$, $y_{\min} \leq y \leq y_{\max}$, and $0 \leq z \leq z_{\max}$ with intervals of Δx, Δy, and Δz, respectively. We set $x_{\min} = -37.0$, $x_{\max} = 37.0$, $y_{\min} = -37.0$, $y_{\max} = 37.0$, $z_{\max} = 100.0$, $\Delta x = 1.0$, $\Delta y = 1.0$, and $\Delta z = 0.1$ cm. The number of voxels in the 3-D images was $75 \times 75 \times 1000 = 5.6 \times 10^6$.

Figures 12 and 13 show the images that were generated using the conventional DAS migration and Kirchhoff migration, which were both processed in the time domain. These images are normalized to the maximum pixel value. It is obvious that the image produced by the Kirchhoff migration is better focused and that the shape of each target is clearly visible, which is consistent with the results reported in [6].

Figures 14 and 15 depict the images obtained using Stolt F-K migration and the hybrid of Kirchhoff migration and Stolt F-K migration that constitutes the proposed method. The image generated using Stolt F-K migration is as blurred as the image generated using the DAS migration, which is understandable because Stolt F-K migration is simply DAS processing that is calculated in the frequency domain. In contrast, the image that was generated using the proposed method shows the target details more clearly than any of the conventional images.

The computation times for the DAS migration, the Kirchhoff migration, Stolt's F-K migration, and the proposed method were 1119.3 s, 1148.8 s, 2.48 s, and 4.49 s, respectively. For this calculation, we used the C language with the SSL2 library (Fujitsu, Japan) running on a computer with an Intel Xeon E5-2650 v2 processor and 32 GB of RAM. The speed of the proposed method is around 250 times faster than both the DAS and Kirchhoff migrations, although Stolt F-K migration is actually 1.8 times faster than the proposed method. From these results, we can conclude that the computation speed of the proposed method is comparable to that of Stolt's F-K migration, whereas the proposed method can produce a clearer image than the conventional methods in this realistic scenario.

IX. Evaluation of Imaging Resolution

In this section, we evaluate the resolutions of each of the imaging methods by applying them to a measured dataset for a metallic target in the form of a Siemens star. The measurement scenario is shown in Fig. 16, and the actual target shape is shown in Fig. 17. All measurement settings are the same as

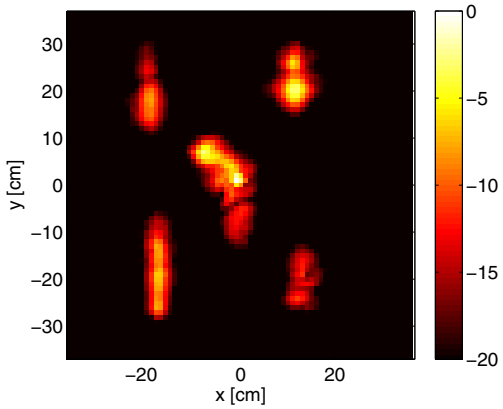

Fig. 15. Image generated using the proposed method (in decibels). The computation time was 4.49 s.

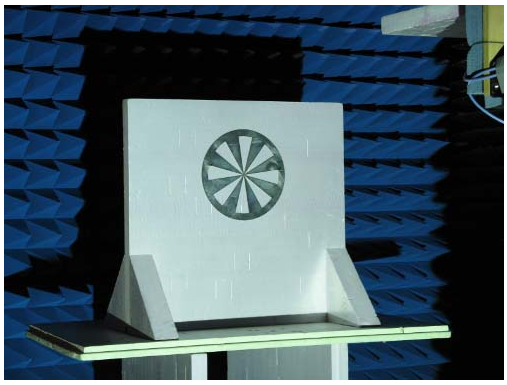

Fig. 16. Photograph of Siemens star-shaped target used in the resolution evaluation.

those used in the previous section. Fig. 18 shows the four images generated using DAS migration, Kirchhoff migration, Stolt F-K migration, and the proposed method. The image that was generated using DAS migration is so severely distorted that it is difficult to define the resolution based on the image, whereas the other three images each have different image resolution values.

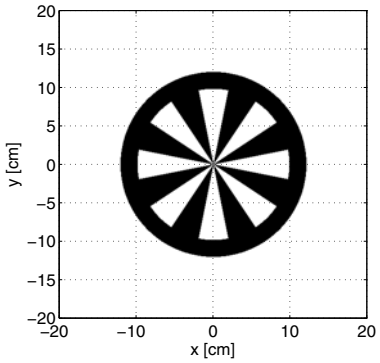

Fig. 17. The actual shape of Siemens star-shaped target. The inner and outer radii are 9.8 cm and 12.0 cm.

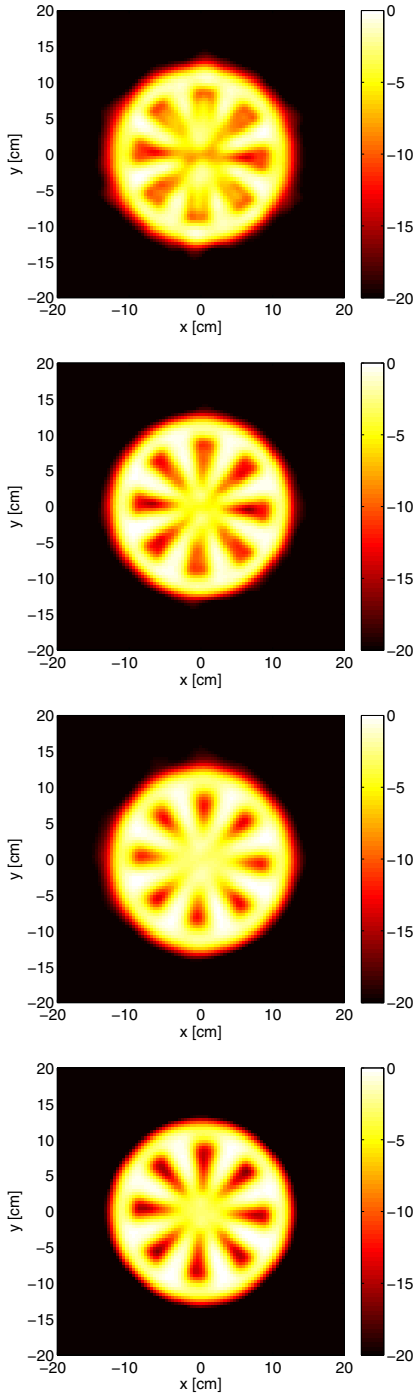

Fig. 18. Images of Siemens star target generated using, from top to bottom, DAS migration, Kirchhoff migration, Stolt FK migration and the proposed method (in decibels).

The spatial resolution of each image is calculated by finding a gap between the adjacent metal sections at a point where the target image strips are merged. The images are normalized to their maximum intensity, and we define the resolution of these images using a threshold of $I_{\mathrm{th}} = -6\mathrm{dB}$. We find the pixels $I(\boldsymbol{r})$ with value I_{th}, and among these pixels, we find the pixel nearest to the center of the target, $\boldsymbol{r}_{\mathrm{c}}$. Because each gap in the Siemens star target has an angle of $\theta_{\mathrm{s}} = \pi/8$, the special

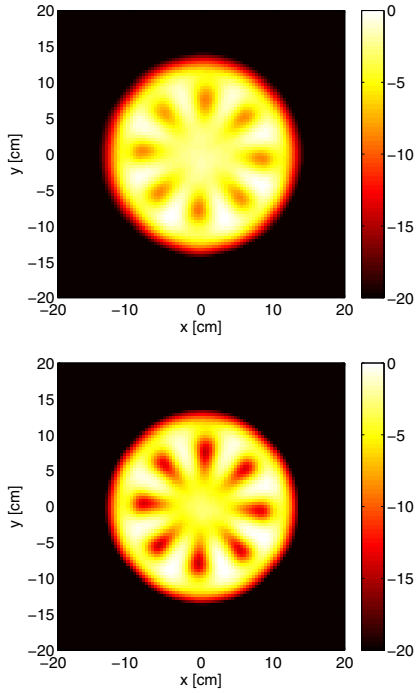

Fig. 19. Images generated using Stolt FK migration (top) and the proposed method (bottom) for a windowing roll off factor $\alpha = 0.8$ (in decibels).

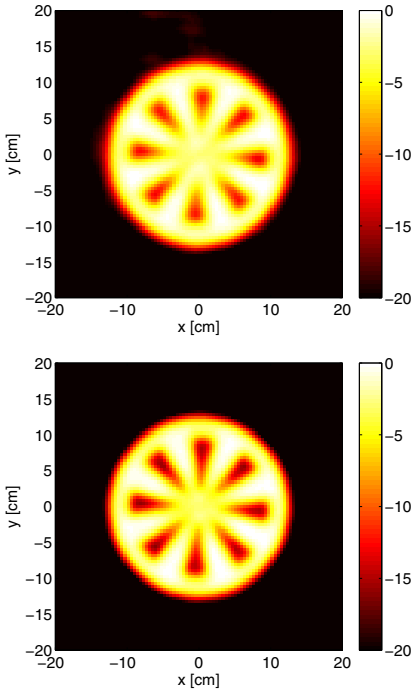

Fig. 20. Images generated using Stolt FK migration (top) and the proposed method (bottom) for a windowing roll off factor $\alpha = 0.0$ (in decibels).

resolution Δr can be expressed approximately as

$$\begin{aligned} &\Delta r = \theta_{\rm s} \min_{\boldsymbol{r}} |\boldsymbol{r} - \boldsymbol{r}_{\rm c}| \\ &\text{subject to } I(\boldsymbol{r}) = I_{\rm th}. \end{aligned} \tag{19}$$

Based on this definition, the values of the spatial resolution Δr were calculated to be 1.34 cm, 0.88 cm and 0.73 cm for Stolt F-K migration, Kirchhoff migration and the proposed method, respectively. These results quantitatively demonstrate the effectiveness of both Kirchhoff migration and our proposed method in terms of imaging resolution.

As noted in Section VI, the roll off factor α has been set to 0.3 above. Because the resolution depends on α, let us show images generated for different values of α. Fig. 19 shows the images produced using Stolt F-K migration and the proposed method for $\alpha = 0.8$, and Fig. 20 shows the same images for $\alpha = 0.0$. From these images, it is learned that the proposed method has a higher resolution than Stolt F-K migration method regardless of a window size. In practice, a window size needs to be properly selected, considering the trade-off between resolution and acceptable artifact level.

X. Discussion

As we mentioned earlier, the number of measurement points was set to be $75 \times 75 = 5625$. The ProVision 2 (L-3 Communications, NY) body scanner, which is currently deployed in numerous airports, is intended to perform measurements at more than 128,000 points (320×400), as calculated based on the array size (2.0 m), the scanning diameter (1.6 m) and the operating frequency (24.0 GHz). Another body scanner that is being developed by Rohde & Schwartz, Germany uses 736 transmitters and 736 receivers, which result in more than 540,000 measurements. In comparison, therefore, the number of measurement points assumed in this paper is not particularly large.

The proposed method was developed by expansion of an existing method (modified Kirchhoff migration). Because modified Kirchhoff migration was successfully applied to a MIMO radar system, it is deduced that our method could also be applied to MIMO radar, although MIMO radar lies outside the scope of this paper.

XI. Conclusion

In this paper, we proposed a fast and accurate imaging algorithm for UWB radar imaging based on a combination of Kirchhoff migration and Stolt's F-K migration. We introduced the texture angle and the IBST to obtain the reflection-point locations, and generated modified Kirchhoff signals that corresponded to the integrand of the Kirchhoff integral. Finally, Stolt F-K migration was applied to the modified Kirchhoff signals to obtain an accurate radar image. The proposed method was compared with the conventional DAS migration, Kirchhoff migration, and Stolt F-K migration by applying these methods to a dataset measured from a trihedral corner reflector to evaluate their approximate PSFs. The resulting images showed that the PSF width of the proposed method was found to be between those of the conventional DAS migration and the Kirchhoff migration. Finally, the four algorithms were applied to a dataset for five different targets to demonstrate the effectiveness of the proposed method in a realistic scenario. The proposed method produced clearer images of five different targets than the conventional methods. In addition, the proposed method can produce an image approximately 250

times faster than both the conventional DAS migration and the Kirchhoff migration.

ACKNOWLEDGEMENT

The authors would like to thank Dr. Timofey Savelyev (Omniradar BV, the Netherlands) for his help and advice with this work. This study was supported in part by the Supporting Program for Interaction-based Initiative Team Studies (SPIRITS), Japan-Netherlands joint development of sleep monitoring technology using ultra-wideband radar, the Japan Society for the Promotion of Science Postdoctoral Fellowships for Research Abroad (high-resolution imaging for human bodies with UWB radar using multipath echoes), the Center of Innovation Program (the last 5X innovation R&D center for a smart, happy, and resilient society), JSPS KAKENHI Grant (No. 25249057 and 15K18077), and the R&D project for expansion of radio spectrum resources for more efficient use of frequency resources for the future (The Ministry of Internal Affairs and Communications, Japan).

REFERENCES

[1] M. Arik, O. B. Akan, "Collaborative mobile target imaging in UWB wireless radar sensor networks," *IEEE Journal on Selected Areas in Communications,* vol. 28, no. 6, pp. 950–961, June, 2010.

[2] Y. Yang and A. E. Fathy, "Development and implementation of a real-time see-through-wall radar system based on FPGA," *IEEE Trans. Geoscience and Remote Sensing,* vol. 47, no. 5, pp. 1270–1280, May 2009.

[3] V. Venkatasubramanian, H. Leung, L. Xiaoxiang, "Chaos UWB Radar for Through-the-Wall Imaging," *IEEE Transactions on Image Processing,* vol. 18, no. 6, pp. 1255–1265, June 2009.

[4] H. F. Abutarboush, M. Klemm, "Signal Selection for Contrast-Enhanced UWB Microwave Radar Imaging With Inhomogeneous Breast Phantoms," *IEEE Antennas and Wireless Propagation Letters,* vol. 12, pp. 1408–1411, 2013.

[5] T. Counts, A. C. Gurbuz, W. R. Scott Jr., J. H. McClellan, and K. Kim, "Multistatic ground-penetrating radar experiments," *IEEE Trans. Geoscience and Remote Sensing,* vol. 45, no. 8, pp. 2544–2553, August 2007.

[6] X. Zhuge, A. G. Yarovoy, T. Savelyev, L. Ligthart, "Modified Kirchhoff migration for UWB MIMO array-based radar imaging," *IEEE Transactions on Geoscience and Remote Sensing,* vol. 48, no. 6, pp. 2692–2703, 2010.

[7] X. Xu, E. L. Miller, C. M. Rappaport, "Minimum entropy regularization in frequency-wavenumber migration to localize subsurface objects," *IEEE Transactions on Geoscience and Remote Sensing,* vol. 41, no. 8, pp. 1804–1812, August 2003.

[8] J.-G. Zhao, M. Sato, "Radar Polarimetry Analysis Applied to Single-Hole Fully Polarimetric Borehole Radar," *IEEE Transactions on Geoscience and Remote Sensing,* vol. 44, no. 12, pp. 3547–3554, December 2006.

[9] D. Garcia, L. L. Tarnec, S. Muth, E. Montagnon, J. Porée, G. Cloutier, "Stolt's f-k migration for plane wave ultrasound imaging," *IEEE Transactions on Ultrasonics, Ferroelectrics and Frequency Control,* vol. 60, no. 9, pp. 1853–1867, September 2013.

[10] C. Gilmore, I. Jeffrey, and J. Lovetri, "Derivation and comparison of SAR and frequency-wavenumber migration within a common inverse scalar wave problem formulation," *IEEE Transactions on Geoscience and Remote Sensing,* vol. 44, no. 6, pp. 1454–1461, June 2006.

[11] J. A. Stratton, *Electromagnetic Theory,* Wiley-IEEE Press, Hoboken, NJ, 2007.

[12] W. Zhang and A. Hoorfar, "Three-dimensional real-time through-the-wall radar imaging with diffraction tomographic algorithm," *IEEE Transactions on Geoscience and Remote Sensing,* vol. 51, no. 7, 2013.

[13] T. Sakamoto, "A fast algorithm for 3-dimensional imaging with UWB pulse radar systems," *IEICE Transactions on Communications,* vol. E90-B, no. 3, pp. 636–644, March 2007.

[14] D. W. Winters, J. D. Shea, E. L. Madsen, G. R. Frank, B. D. Van Veen, S. C. Hagness, "Estimating the Breast Surface Using UWB Microwave Monostatic Backscatter Measurements," *IEEE Transactions on Biomedical Engineering,* vol. 55, no. 1, pp. 247–256, January 2008.

[15] S. Hantscher, A. Reisenzahn, C. G. Diskus, "Through-Wall Imaging With a 3-D UWB SAR Algorithm," *IEEE Signal Processing Letters,* vol. 15, pp. 269–272, February 2008.

[16] R. Salman, I. Willms, "In-Wall Object Recognition based on SAR-like Imaging by UWB-Radar," *Proc. 8th European Conference on Synthetic Aperture Radar (EUSAR),* June 2010.

[17] S. Kidera, Y. Kani, T. Sakamoto, T. Sato, "A fast and high-resolution 3-D imaging algorithm with linear array antennas for UWB pulse radars," *IEICE Transactions on Communications,* vol. E91-B, no. 8, pp. 2683–2691, August 2008.

[18] T. Sakamoto, T. G. Savelyev, P. J. Aubry, and A. G. Yarovoy, "Revised Range Point Migration Method for Rapid 3-D Imaging with UWB Radar," *Proc. 2012 IEEE International Symposium on Antennas and Propagation and USNC-URSI National Radio Science Meeting,* July 2012.

[19] T. Sakamoto, T. Sato, Y. He, P. J. Aubry, A. G. Yarovoy, "Texture-based technique for separating echoes from people walking in UWB radar signals," *Proc. 2013 URSI International Symposium on Electromagnetic Theory (EMTS),* pp. 119–122, 2013.

[20] T. Sakamoto, T. Sato, P. J. Aubry, and A. G. Yarovoy, "Texture-based automatic separation of echoes from distributed moving targets in UWB radar signals," *IEEE Trans. on Geoscience and Remote Sensing,* vol. 53, no. 1, pp. 352–361, 2015.

PLACE PHOTO HERE

Takuya Sakamoto (M'04) received the B.E. degree from Kyoto University, Kyoto, Japan, in 2000 and the M.I. and Ph.D. degrees from the Graduate School of Informatics, Kyoto University, in 2002 and 2005, respectively.

Since 2015, he has been an Associate Professor at the Graduate School of Engineering, University of Hyogo. From 2006 through 2015, he was an Assistant Professor at the Graduate School of Informatics, Kyoto University. From 2011 through 2013, he was a Visiting Researcher in Microwave Sensing, Signals and Systems, Delft University of Technology (TUD), Delft, The Netherlands. During this period, he worked as a member of the European Union's ATOM project (for airport detection and tracking of dangerous materials by passive and active sensors arrays). His current research interests lie in ultrawideband radar, radar imaging, and radar signal processing.

Dr. Sakamoto is a member of the Institute of Electronics, Information and Communication Engineers of Japan (IEICE), the Institute of Electrical Engineers of Japan (IEEJ), and the Japan Society of Ultrasonics in Medicine. He received the Best Paper Award from the International Symposium on Antennas and Propagation (ISAP2004) in 2004, the Young Researcher's Award from the IEICE in 2007, the Best Presentation Award from the IEEJ in 2007, the Best Paper Award from the IEICE Communication Society in 2007, and the Best Paper Award from the International Symposium on Antennas and Propagation (ISAP2012) in 2012.

PLACE PHOTO HERE

Toru Sato (M'92) received the B.E., M.E., and Ph.D. degrees in electrical engineering from Kyoto University, Kyoto, Japan, in 1976, 1978, and 1982, respectively.

He has been with Kyoto University since 1983 and is currently a Professor in the Department of Communications and Computer Engineering in the Graduate School of Informatics. His major research interests have included system design and signal processing aspects of atmospheric radar, radar remote sensing of the atmosphere, observations of precipitation using radar and satellite signals, radar observation of space debris, and signal processing for subsurface radar signals.

Prof. Sato is a member of the Institute of Electronics, Information, and Communication Engineers of Japan, the Society of Geomagnetism and Earth, Planetary and Space Sciences, the Japan Society for Aeronautical and Space Sciences, the Institute of Electrical and Electronics Engineers, and the American Meteorological Society. He was awarded the Tanakadate Prize in 1986.

PLACE PHOTO HERE

Pascal J. Aubry received the D.E.S.S. degree in electronics and automatics from the Université Pierre et Marie Curie (Paris 6), Paris, France, in 1993.

He was a Young Graduate Trainee with the European Space Research and Technology Centre (ESTEC) in 1996, where he was involved in antenna measurements. Since 1997, he has been with the International Research Centre for Telecommunications and Radar, Delft University of Technology (TUD), Delft, The Netherlands. His research interests include antenna measurement techniques, radar system testing, and signal processing and analysis.

PLACE PHOTO HERE

Alexander G. Yarovoy (M'96-SM'04) received the Diploma (with honor) in radiophysics and electronics from the Kharkov State University, Kharkov, Ukraine, in 1984. He received the Candidate Phys. & Math. Sci. and Doctor Phys. & Math. Sci. degrees in radiophysics from the Kharkov State University, Kharkov, Ukraine in 1987 and 1994, respectively.

In 1987, he joined the Department of Radiophysics at the Kharkov State University as a Researcher and became a Professor there in 1997. From September 1994 through 1996, he was with the Technical University of Ilmenau, Ilmenau, Germany, as a Visiting Researcher. Since 1999, he has been with the Delft University of Technology, Delft, The Netherlands. Since 2009, he has been the Chair of Microwave Sensing, Systems and Signals. His main research interests are in ultrawideband (UWB) microwave technology and its applications (particularly radar) and applied electromagnetics (particularly UWB antennas). He has authored and coauthored more than 250 scientific or technical papers, four patents, and 14 book chapters.

Prof. Yarovoy served as a Guest Editor for five special issues of IEEE Transactions and other journals. Since 2011, he has been an Associated Editor of the International Journal of Microwave and Wireless Technologies. He was the recipient of the European Microwave Week Radar Award for the paper that best advances the state-of-the-art in radar technology in 2001 (together with L. P. Ligthart and P. van Genderen) and again in 2012 (together with T. Savelyev). In 2010, together with D. Caratelli, he received the Best Paper Award from the Applied Computational Electromagnetic Society. He served as the Chair and Technical Program Committee Chair of the 5th European Radar Conference (EuRAD'08), Amsterdam, The Netherlands, as well as the Secretary of the 1st European Radar Conference (EuRAD'04), Amsterdam. He served also as the Cochair and TPC Chair of the 10th International Conference on GPR (GPR2004) in Delft. Since 2008, he has served as the Director of the European Microwave Association.